

Effect of patterned hydrodynamic slip on electromagnetohydrodynamic flow in parallel plate microchannel

Chun-Hong Yang(杨春红), Yong-Jun Jian(菅永军)

Citation: Chin. Phys. B . 2020, 29(11): 114101 . **doi:** 10.1088/1674-1056/abab71
Journal homepage: http://cpb.iphy.ac.cn; http://iopscience.iop.org/cpb

What follows is a list of articles you may be interested in

Superconducting membrane mechanical oscillator based on vacuum-gap capacitor

Yong-Chao Li(李永超), Xin Dai(戴欣), Jun-Liang Jiang(江俊良), Jia-Zheng Pan(潘佳政), Xing-Yu Wei(魏兴雨), Ya-Peng Lu(卢亚鹏), Sheng Lu(卢盛), Xue-Cou Tu(涂学凑), Guo-Zhu Sun(孙国柱), Pei-Heng Wu(吴培亨)

Chin. Phys. B . 2018, 27(6): 060701 . **doi:** 10.1088/1674-1056/27/6/060701

Design and characterization of a 3D encapsulation with silicon vias for radio frequency micro-electromechanical system resonator

Ji-Cong Zhao(赵继聪), Quan Yuan(袁泉), Feng-Xiang Wang(王凤祥), Xiao Kan(阚骁), Guo-Wei Han(韩国威), Ling Sun(孙玲), Hai-Yan Sun(孙海燕), Jin-Ling Yang(杨晋玲), Fu-Hua Yang(杨富华)

Chin. Phys. B . 2017, 26(6): 060705 . **doi:** 10.1088/1674-1056/26/6/060705

Uniform stable conformal convolutional perfectly matched layer for enlarged cell technique conformal finite-difference time-domain method

Wang Yue, Wang Jian-Guo, Chen Zai-Gao

Chin. Phys. B . 2015, 24(2): 024101 . **doi:** 10.1088/1674-1056/24/2/024101

Finger capacitance of a terahertz photomixer in low-temperature-grown GaAs using the finite element method

Chen Long-Chao, Fan Wen-Hui

Chin. Phys. B . 2012, 21(10): 104101 . **doi:** 10.1088/1674-1056/21/10/104101

Effect of patterned hydrodynamic slip on electromagnetohydrodynamic flow in parallel plate microchannel*

Chun-Hong Yang(杨春红) and Yong-Jun Jian(菅永军)†

School of Mathematical Science, Inner Mongolia University, Hohhot 010021, *China*

(Received 3 April 2020; revised manuscript received 24 May 2020; accepted manuscript online 1 August 2020)

A fully developed electromagnetohydrodynamic (EMHD) flow through a microchannel with patterned hydrodynamic slippage on the channel wall is studied. The flow is driven by the Lorentz force which originates from the interaction between an externally imposed lateral electric field and a perpendicular magnetic field. The governing equations for the velocity with patterned slip boundary conditions are solved analytically by perturbation techniques under the assumption of small Reynolds number *Re*. In addition, the numerical solutions for the velocity are obtained by using the finite-difference method, and they are found to be in good agreement with the analytical solutions within admissible parameter range. The effects of different parameters on the velocity and volume flow rate due to patterned hydrodynamic slippage are discussed in detail, including wave-number K, Hartmann number Ha, amplitude δ of the patterned slip length, and normalized electric field strength S. The results show that patterned slippage over microchannel walls can induce transverse flows, which will increase the mixing rates in microfluidic devices. In addition, we also find that precise flow control can be achieved by controlling the magnetic flux and the wave-number and also by well choosing the electric field intensity. Our analysis can be used for designing the efficient micro-fluidic mixers.

Keywords: electromagnetohydrodynamic (EMHD) flow, patterned slip wall

PACS: 41.20.Cv, 62.10.+s, 07.10.Cm, 52.30.Cv **DOI:** 10.1088/1674-1056/abab71

1. Introduction

In recent years, with the increasing applications of microfluids and nanofluids, the microscale transport, mixing and sorting process have found rather a wild application in micro-electro-mechanical systems (MEMS), biochemical, chemical, and medical fields.[1–5] As the scale of the device diminishes, driving the fluid flow in such devices becomes more difficult. The magnetic field is one of the important actuation mechanisms in microchannels due to its wide applications in engineering and biomedical fields, and it has several advantages such as no moving part, easy-to-fabricate, low-voltage operation, adjustable movement direction, and able-to-achieve relatively high flow rate.[6–8] The driving force in the electromagnetohydrodynamic (EMHD) micropumps is the Lorentz force generated by the interaction between an externally imposed lateral electric field and a vertical magnetic field. Numerous theoretical and experimental researches on the analysis of the behaviors of magnetohydrodynamic (MHD) and EMHD micropumps have been carried out.[9–12] Experiments conducted by Jang and Lee[13] proved the effectiveness of increasing flow rates of microchannel under the action of a low-magnitude magnetic field. Jian *et al.*[14] analytically studied the transient rotating EMHD flow for both direct current (DC) and alternating current (AC) electric field through a parallel microchannel. Wang *et al.*[15] numerically analyzed a two-dimensional fully developed MHD flow and concluded that the induced Lorentz force had great influence on the flow velocity field.

It seems that recent discussion about MHD micro-pumps did not consider the slip effect on the fluid velocity, in which the velocity is usually assumed to vanish at the wall. No slip condition implies a perfect wettability at the liquid-solid interface, which is valid in most normal scale fluid flow problems. However, with the development of research on microscale fluids, it is increasingly realized that the classical non-slip boundary conditions are not always applicable. Instead, the slip effect is common in many microfluidic and nanofluidic applications.[16,17] Fluid slippage is usually described in terms of a slip length, which is characterized by the distance between the solid surface and the hypothetical solid surface on which the slip velocity decreases linearly to zero. The main reason for the origin of slippage is believed to be the nanobubbles trapped on the hydrophobic surface.[18] In addition, there are other factors that affect the slippage significantly, they including surface contamination and surface roughness.[18] The existing experimental data show that the slip length can be taken in a range from nanometer to micrometer,[19,20] which accords with the micro-devices size we discuss. That is why we need to discuss the effect of hydrodynamic slippage on microfluidic flows. Further, this effect can be used to overcome some disadvantages of microfluidic laminar flows. Rivero and

*Project supported by the National Natural Science Foundation of China (Grant Nos. 11772162 and 11472140), the Natural Science Foundation of Inner Mongolia Autonomous Region, China (Grant Nos. 2016MS0106 and 2018MS01015), and the Inner Mongolia Grassland Talent, China (Grant No. 12000-12102013).

†Corresponding author. E-mail: jianyj@imu.edu.cn

© 2020 Chinese Physical Society and IOP Publishing Ltd

Cuevas[21] analyzed the influence of constant slip condition on the MHD flow in a rectangular microchannel.

In all the above-mentioned investigations, the researchers have developed their models under the assumption of the homogenous hydrodynamic slippage, *i.e.*, the effective slip length is a constant everywhere on the surfaces. However, inhomogeneous hydrophobic surfaces could also lead to patterned hydrodynamic slip on the solid walls.[22,23] Owing to the strong relationship between wettability and slip,[24,25] patterned wettability can be used to induce variations in slip, which can induce transverse or circulating flows in channel.[26] The presence of this patterned hydrodynamic slip can result in the enhancement of the efficiency of the micro-mixing, which has aroused the interest of many experts. According to the molecular dynamics simulations, Hendy *et al.*[26] have conceived a micro-mixer and proved that patterned slip could effectively induce mixing in flow. Zhao *et al.*[27] first studied the electro-osmotic flow with patterned slip condition at the channel wall and concluded that the patterned slip condition can induce complex flow model. The effect of patterned slippage on the flow of non-Newtonian fluid was discussed later.[28] Their results showed that for shear-thickening fluids, significant transverse flows comparable in size with those produced for Newtonian fluids would be induced by patterned slip effect. The effect of patterned surface on the flow vortices combined with substrate wettability was discussed by Mayur *et al.*[29] in a nanometer range. In fact, the slip behaviors and its variation with interface property of simple liquid on solid surface are still a controversial issue.[30,31] More and more efforts have been devoted to the study of the effects of slip conditions on flow properties in micro-fluidics, which has wide applications in biochemical and chemical synthesis.[32,33]

The aim of our study is to discuss the EMHD flow through a parallel plate microchannel under a patterned slip boundary condition by assuming that the slip length varies in space. We consider the cosine wave variations in the slip length. First, the perturbation technique is used to derive the analytical solutions of flow velocity and volume flow rate under the condition of low Reynolds number *Re*, and these analytical solutions are compared with the numerical solutions obtained by the finite-difference method. Then the influences of several normalized parameters on velocities and volume flow rates are determined graphically. Our theoretical results may provide some guidances for designing the mixers in microchannels.

2. Formulation of problem

2.1. Physical model and explanation of problem

Taking a patterned slip length on wall into consideration, we investigate a fully developed EMHD flow of an incompressible electrically conducting fluid between two parallel plates. In our analysis, the induced magnetic field is ignored due to the small enough magnetic Reynolds number. The physical model and the coordinate system are shown in Fig. 1. The original point of Cartesian coordinate system (x^*, y^*, z^*) is located at the middle of channel. The channel height and length are $2H$ (in the y^* direction) and L (in the x^* direction) respectively. An external electric field E is applied along the z^* axis, and a uniform magnetic field B is applied perpendicular to the plates. The flow is driven by the axial Lorentz force produced by the interaction of the externally applied electric field and magnetic field. We assume that the channel length L is much longer than the channel height $2H$, *i.e.*, $L \gg 2H$. The flow considered in the present study is steady and fully developed, which is compatible with low-Reynolds number flows.

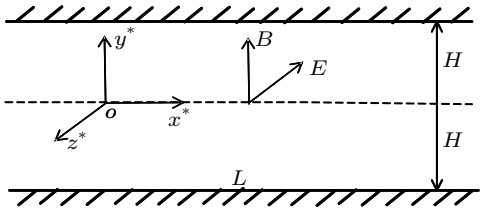


Fig. 1. Schematic diagram of physical modeling.

2.2. Flow analysis and mathematical formulation

For a fully developed EMHD flow considered in this paper, the velocity is governed by the continuity equation and the momentum equation written as

$$\nabla \cdot \boldsymbol{u}^* = 0, \tag{1}$$

$$\rho\left(\frac{\partial \boldsymbol{u}^*}{\partial t^*} + (\boldsymbol{u}^* \cdot \nabla)\boldsymbol{u}^*\right) = -\nabla p^* + \mu \nabla^2 \boldsymbol{u}^* + \boldsymbol{F}, \tag{2}$$

where ρ is the density of fluid, $\mu = \rho\gamma$ is the dynamic viscosity of fluid, $\boldsymbol{u}^* = (u^*, v^*, 0)$ is the velocity, ∇p^* is the pressure difference along the channel, and $\boldsymbol{F} = \boldsymbol{J} \times \boldsymbol{B}$ is the Lorentz force along the channel. Using Ohm's law,[34] we obtain the expression of the local ion current density $\boldsymbol{J} = \sigma(\boldsymbol{E} + \boldsymbol{u}^* \times \boldsymbol{B})$, where σ is the electrical conductivity and $\boldsymbol{B} = (0, B_y, 0)$. Further, we can obtain the component forms of the above Eqs. (1) and (2) as

$$\frac{\partial u^*}{\partial x^*} + \frac{\partial v^*}{\partial y^*} = 0, \tag{3}$$

$$\mu\left(\frac{\partial^2 u^*}{\partial x^{*2}} + \frac{\partial^2 u^*}{\partial y^{*2}}\right) - \frac{\partial p^*}{\partial x^*} - \rho\left(u^*\frac{\partial u^*}{\partial x^*} + v^*\frac{\partial u^*}{\partial y^*}\right) + \sigma(B_y E - B_y^2 u^*) = 0, \tag{4}$$

$$\mu\left(\frac{\partial^2 v^*}{\partial x^{*2}} + \frac{\partial^2 v^*}{\partial y^{*2}}\right) - \frac{\partial p^*}{\partial y^*} - \rho\left(u^*\frac{\partial v^*}{\partial x^*} + v^*\frac{\partial v^*}{\partial y^*}\right) = 0, \tag{5}$$

$$\frac{\partial p^*}{\partial z^*} = 0. \tag{6}$$

The patterned slip boundary conditions on the channel walls for the axial velocity component u^*, which is well-known as

Navier slip boundary condition,[35] and no-penetration conditions for the transverse velocity component v^* are written as

$$u^*\big|_{y^*=H} = -\delta^*(x^*)\frac{\partial u^*}{\partial y^*}\Big|_{y^*=H}, \tag{7}$$

$$u^*\big|_{y^*=-H} = \delta^*(x^*)\frac{\partial u^*}{\partial y^*}\Big|_{y^*=-H}, \tag{8}$$

$$v^*\big|_{y^*=H} = 0, \quad v^*\big|_{y^*=-H} = 0, \tag{9}$$

where $\delta^*(x^*)$ is the slip length physically describing hydrodynamic slip effect. In our analysis, we suppose $\delta^*(x^*) = \delta_0(1+\alpha\,\mathrm{e}^{\mathrm{i}kx*})$, which varies periodically with the axial location. It should be pointed out that the common non-slip condition corresponds to the case of $\delta_0 = 0$ in our analysis.

The following non-dimensional variables are introduced:

$$\begin{aligned}
&u = \frac{u^*}{U}, \quad v = \frac{v^*}{U}, \quad p = \frac{p^*}{P_0}, \quad x = \frac{x^*}{H},\\
&y = \frac{y^*}{H}, \quad U = \frac{\gamma}{H}, \quad \delta = \frac{\delta_0}{H},\\
&P_0 = \frac{\mu U}{H}, \quad S = \frac{EH}{U}\sqrt{\frac{\sigma}{\mu}}, \quad Ha = B_y H\sqrt{\frac{\sigma}{\mu}},\\
&Re = \frac{\rho U H}{\mu}, \quad K = kH,
\end{aligned} \tag{10}$$

where $\gamma = \mu/\rho$ is the kinematic viscosity coefficient, Ha is the Hartman number representing the relative strength of the electromagnetic forces and the viscous forces, and S is a non-dimensional quantity denoting the strength of the lateral electric field. In addition, Re is the Reynolds number, δ is the non-dimensional slip length, and K is the wave-number. Utilizing the non-dimensional variables defined above, the dimensionless governing equations and the corresponding boundary conditions can be rewritten as

$$\frac{\partial u}{\partial x} + \frac{\partial v}{\partial y} = 0, \tag{11}$$

$$\frac{\partial^2 u}{\partial x^2} + \frac{\partial^2 u}{\partial y^2} - Re\left(u\frac{\partial u}{\partial x} + v\frac{\partial u}{\partial y}\right) - \frac{\partial p}{\partial x} + HaS - Ha^2 u = 0, \tag{12}$$

$$\frac{\partial^2 v}{\partial x^2} + \frac{\partial^2 v}{\partial y^2} - Re\left(u\frac{\partial v}{\partial x} + v\frac{\partial v}{\partial y}\right) - \frac{\partial p}{\partial y} = 0, \tag{13}$$

$$u\big|_{y=1} = -\delta(1+\alpha\,\mathrm{e}^{\mathrm{i}Kx})\frac{\partial u}{\partial y}\Big|_{y=1}, \tag{14}$$

$$u\big|_{y=-1} = \delta(1+\alpha\,\mathrm{e}^{\mathrm{i}Kx})\frac{\partial u}{\partial y}\Big|_{y=-1}, \tag{15}$$

$$v\big|_{y=1} = 0,\ v\big|_{y=-1} = 0. \tag{16}$$

In order to solve the above problem analytically, we suppose that the variation of slip length along the axial direction is very small, (*i.e.*, $\alpha \ll 1$), and a regular perturbation approach is applied. For a given physical variable ξ, it can be expanded in the form of power series as

$$\xi = \xi_0 + \alpha\xi_1 + o(\alpha^2), \tag{17}$$

where ξ can be the variables u, v, p.

The zero-order velocity v_0 is zero, and u_0 satisfies the following equations:

$$\frac{\mathrm{d}^2 u_0}{\mathrm{d}y^2} = \frac{\Delta p}{L} - HaS + Ha^2 u_0, \tag{18}$$

$$\frac{\partial p_0}{\partial y} = 0, \tag{19}$$

$$u_0\big|_{y=\pm1} = \mp\delta\frac{\mathrm{d}u_0}{\mathrm{d}y}\Big|_{y=\pm1}, \tag{20}$$

where zero-order pressure gradient has been assumed to be constant without loss of generality, *i.e.*, $\partial p_0/\partial x = \Delta p/L = \Omega$. The solution to Eq. (18) with the boundary condition Eq. (20) can easily be solved and is given below:

$$u_0(y) = \frac{HaS - \Omega}{Ha^2}\left(1 - \frac{\cosh(Hay)}{\cosh(Ha) + \delta Ha\sinh(Ha)}\right), \tag{21}$$

$$v_0 = 0. \tag{22}$$

The governing equations and the corresponding boundary conditions for first-order velocities u_1 and v_1 can be expressed as

$$\frac{\partial u_1}{\partial x} + \frac{\partial v_1}{\partial y} = 0, \tag{23}$$

$$\frac{\partial^2 u_1}{\partial x^2} + \frac{\partial^2 u_1}{\partial y^2} - Re\left(u_0\frac{\partial u_1}{\partial x} + v_1\frac{\mathrm{d}u_0}{\mathrm{d}y}\right) = \frac{\partial p_1}{\partial x} + Ha^2 u_1, \tag{24}$$

$$\frac{\partial^2 v_1}{\partial x^2} + \frac{\partial^2 v_1}{\partial y^2} - Reu_0\frac{\partial v_1}{\partial x} = \frac{\partial p_1}{\partial y}, \tag{25}$$

$$u_1\big|_{y=1} = -\delta\,\mathrm{e}^{\mathrm{i}Kx}\frac{\mathrm{d}u_0}{\mathrm{d}y}\Big|_{y=1} - \delta\frac{\partial u_1}{\partial y}\Big|_{y=1}, \tag{26}$$

$$u_1\big|_{y=-1} = \delta\,\mathrm{e}^{\mathrm{i}Kx}\frac{\mathrm{d}u_0}{\mathrm{d}y}\Big|_{y=-1} + \delta\frac{\partial u_1}{\partial y}\Big|_{y=-1}, \tag{27}$$

$$v_1\big|_{y=1} = 0, v_1\big|_{y=-1} = 0. \tag{28}$$

By examining the form of the boundary condition in Eqs. (26) and (27), we can suppose $u_1 = \mathrm{e}^{\mathrm{i}Kx}f(y)$. Inserting this solution into Eq. (23), we can obtain the form of solution for the transverse velocity to be

$$v_1 = -\mathrm{i}K\,\mathrm{e}^{\mathrm{i}Kx}h(y), \tag{29}$$

where $h'(y) = f(y)$ and $h(0) = 0$ due to the symmetry condition $v_1(0) = 0$.

After eliminating p_1 from Eqs. (24) and (25), we can obtain the following fourth-order ordinary differential equation of $h(y)$:

$$h^{(4)}(y) - (2K^2 + Ha^2 + \mathrm{i}KReu_0)h''(y) + \left(K^4 + \mathrm{i}KRe\frac{\mathrm{d}^2 u_0}{\mathrm{d}y^2} + \mathrm{i}K^3 Reu_0\right)h(y) = 0. \tag{30}$$

Thus the boundary conditions (26) and (27) become

$$h'(y)\big|_{y=\pm1} = \mp\delta u_0'(y)\big|_{y=\pm1} \mp \delta h''(y)\big|_{y=\pm1}, \tag{31}$$

It can be seen that equation (30) is not possible to find an analytical solution when non-constant slip boundary conditions

are all taken into consideration. By resorting to the finite-difference method, the fourth-order ordinary differential equation (30) with boundary condition (31) is numerically solved. Meanwhile, it should be noted that the Reynolds number Re in our analysis is very small, *i.e.*, $Re \ll 1$, so we can simplify Eq. (30) to obtain an analytical solution of $h(y)$ as follows:

$$h^{(4)}(y) - (2K^2 + Ha^2)h''(y) + K^4 h(y) = 0. \tag{32}$$

Substituting the expression of u_0, *i.e.*, Eq. (21) into the boundary condition (31), we can obtain the solution of Eq. (32)

$$h(y) = D_1 \sinh(\lambda_1 y) + D_2 \sinh(\lambda_2 y), \tag{33}$$

where

$$\begin{aligned}
\lambda_1 &= \sqrt{\frac{(2K^2 + Ha^2) + Ha\sqrt{4K^2 + Ha^2}}{2}}, \\
\lambda_2 &= \sqrt{\frac{(2K^2 + Ha^2) - Ha\sqrt{4K^2 + Ha^2}}{2}}, \\
D_1 &= \frac{\delta(HaS - \Omega)E_1}{Ha^2(E_2 + \delta E_3)}, \quad D_2 = -\frac{\sinh\lambda_1}{\sinh\lambda_2} D_1, \\
E_1 &= \frac{Ha\sinh(Ha)}{\cosh(Ha) + \delta Ha\sinh(Ha)}, \\
E_2 &= \lambda_1 \cosh\lambda_1 - \lambda_2 \frac{\sinh\lambda_1 \cosh\lambda_2}{\sinh\lambda_2}, \\
E_3 &= \lambda_1^2 \sinh\lambda_1 - \lambda_2^2 \sinh\lambda_1.
\end{aligned} \tag{34}$$

Then, two components of the first-order velocities u_1, v_1 can be calculated to be

$$u_1 = \mathrm{e}^{\mathrm{i}Kx} h'(y) \quad \text{and} \quad v_1 = -\mathrm{i}K\,\mathrm{e}^{\mathrm{i}Kx} h(y). \tag{35}$$

3. Results and discussion

In the previous sections, we have obtained the velocity profiles of EMHD flow with patterned slippage between two parallel micro-plates. Before we proceed any further, the ranges of relevant parameters used in conventional microfluidic flow should be evaluated. According to the work given in Ref. [36], the half height of the microchannel is $H \sim 10$ μm, the cosine wavelength of slip variation is $k^{-1} \sim 10$ μm, the slip length is $\delta_0 \sim 1$ μm, the density of fluid is $\rho \times 10^3$ kg/m^3, electrical conductivity is $\sigma \sim 2.2 \times 10^{-4}$ S/m–4×10^6 S/m, viscosity is $\mu \sim 10^{-3}$ kg/(m·s)–1.5×10^{-3} kg/(m·s), and the magnitude of the magnetic field strength B_y is 0 T–0.44 T.[37] Hence, the maximum of Hartmann number Ha is no more than 5. In our study, we set the dimensionless slip length to vary from 0.01 to 0.1. The effects of the corresponding parameters on flow field are investigated below.

Figures 2(a) and 2(b) clearly show the contour plots for first order axial velocity u_1 and vertical velocity v_1 in a period of cosine wave variation of slip length. From Fig. 2(a) we can observe that the positive and negative values of axial slip velocity on both channel walls are related to the positive and negative values of slip length. There are two zero points in the slip length, at which the slip velocity u_1 values both vanish. The direction of axial flow near the plate is opposite to that far from the plate. It is shown in Fig. 2(b) that in the first half of the slip length, the transverse flow moves from the two channel wall to the center of the channel, while the case is opposite in the second half. This result is similar to the conclusions obtained in Ref. [27].

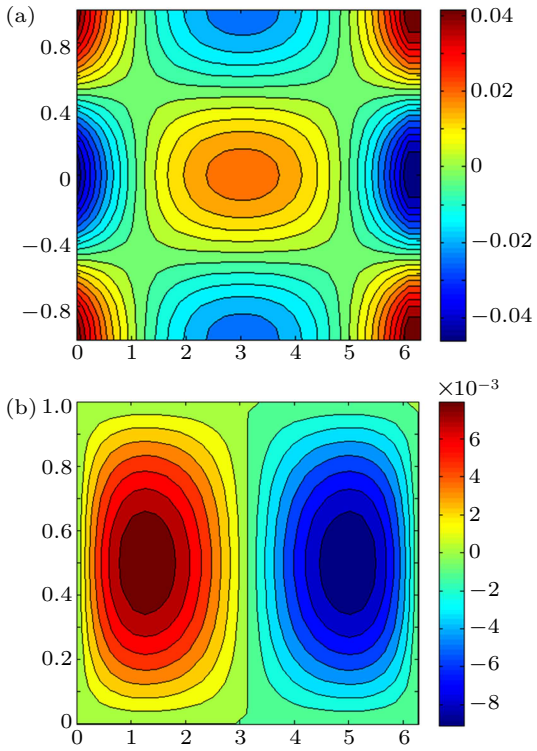


Fig. 2. Contours plots for dimensionless velocity variations of (a) axial velocity u_1, (b) vertical velocity v_1 with a cosine wave variation in slip length on wall at $Re = 0.01$, $Ha = 1$, $S = 1$, $\Omega = 0$, $\delta = 0.1$, and $K = 1$.

Without losing generality, we ignore the complex unit i in the expression of vertical velocity v_1 in the following graphical results. Meanwhile, in order to validate our analytical solutions of slip velocity, comparisons with the numerical solutions for slip velocity is conducted. In the following graphs we use line graphs to represent the analytical results and point graphs to represent the numerical results.

Figure 3 shows the distributions of slip velocity for different wave-number K. We can see that the analytical solutions and the numerical solutions are in excellent agreement. It is clearly shown in Fig. 3(a) that the absolute value of axial velocity mainly decreases with the increase of K, and whose profile is flatter for bigger K. Besides, the direction of axial slip velocity changes probably at $y = \pm 0.5$. In Fig. 3(b), the transverse velocity is opposite in the upper half and lower half of the board. Although the magnitude of vertical velocity v_1 is very small, we can still see that the magnitude of vertical

velocity increases with the increase of K. Mathematically, the reason for this phenomena is that the transverse velocity v_1 is proportional to K, which can be seen in Eq. (35). Physically, the longitudinal energy will be enhanced with the increase of vertical velocity, ultimately resulting in the decrease of horizontal velocity. Therefore, the important prediction is that the increase of K can induce a significant transverse velocity while the flow is suppressed in the axial direction.

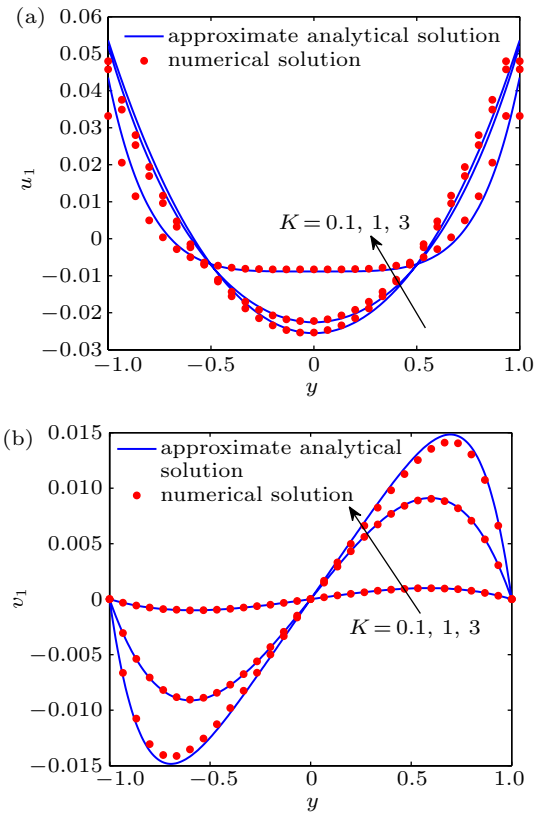


Fig. 3. Comparison between analytical and numerical solutions for the first-order (a) axial velocity u_1 and (b) vertical velocity v_1 at three different values of wave-number K ($x = 0.0628$, $Re = 0.01$, $Ha = 1$, $S = 1$, $\Omega = 0$, $\delta = 0.1$).

Next, in Fig. 4 we consider the effect of varying slip length δ on slip velocity with $K = 1$. Note that $\delta = 0$ means the case of no slip on the micro-channel wall, so both horizontal and vertical first-order velocity components are equal to 0. Besides, in Fig. 4(a) the absolute value of axial slip velocity shows an increasing trend with δ, and the direction of velocity in the center of the plate is opposite to that near the microchannel wall. The variation trend of the vertical slip velocity in Fig. 4(b) is similar to that in Fig. 3(b), which provides the possibility to produce vortex. The result can be explained by the fact that the leading order terms of slip velocity in two directions are proportional to δ.

Figure 5 illustrates the variations of slip velocity with Hartmann number Ha. From Figs. 5(a) and 5(b), it can be observed that both velocities in two directions decrease monotonically with the increase of Hartmann number, which indicates that Ha acts as an brake to the velocity field. The reason is that the increase of Ha induces the Lorentz force to increase, which results in the decrease of the velocity.

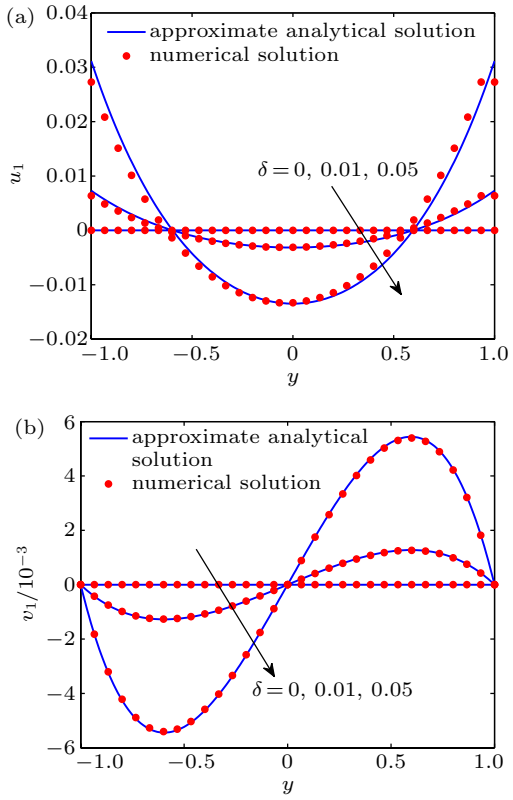


Fig. 4. First-order velocity distributions for different values of non-dimensional slip length δ at $K = 1$ ($x = 0.0628$, $Re = 0.01$, $Ha = 1$, $S = 1$, $\Omega = 0$), sowing (a) axial velocity u_1 and (b) vertical velocity v_1 varying with y.

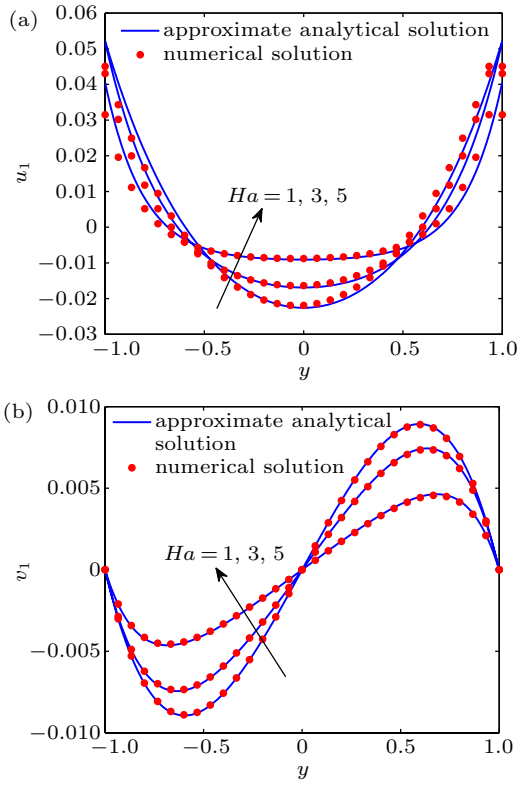


Fig. 5. First-order velocity distributions for different values of Hartmann number Ha ($x = 0.2096$, $Re = 0.01$, $S = 1$, $\Omega = 0$, $K = 1$, $\delta = 0.1$, $\alpha = 0.01$), showing (a) axial velocity u_1 and (b) vertical velocity v_1 *versus* y.

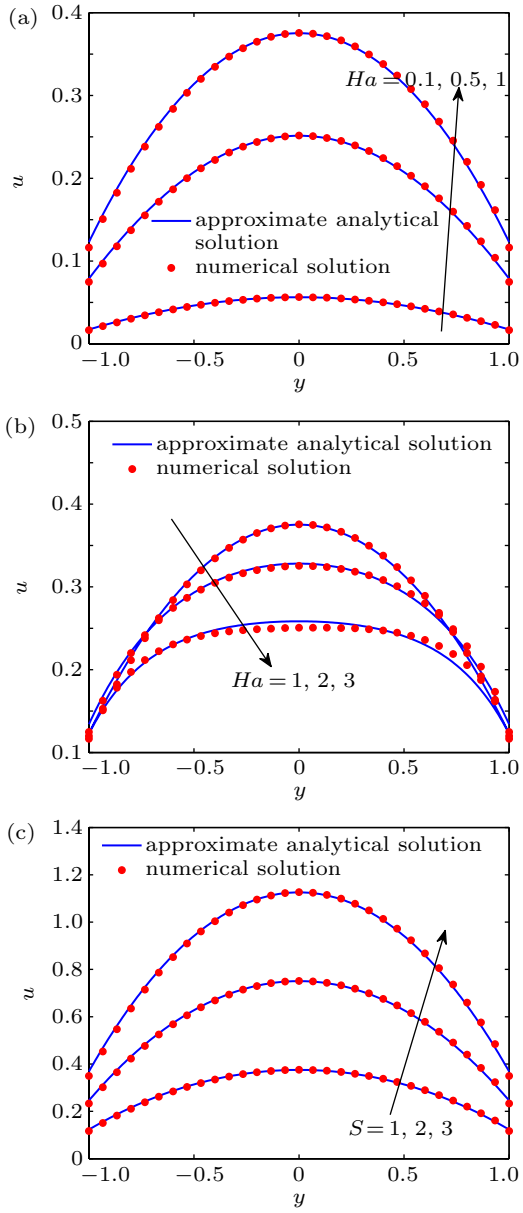


Fig. 6. Variations of total axial velocity $u = u_0 + \alpha u_1$ with y for different values of Hartmann number Ha and electric field strength S: [(a), (b)] $S = 1$ and (c) $Ha = 0.1$ at $x = 0.2096$, $Re = 0.01$, $\Omega = 0$, $K = 1$, $\delta = 0.1$, $\alpha = 0.01$.

The variations of total axial velocity with y for different values of Hartmann number Ha and normalized electric field strength S are discussed in Fig. 6. Here, the total axial velocity is the combination of zero-order and first-order axial velocity, *i.e.*, $u = u_0 + \alpha u_1$, where $\alpha = 0.01$. It is worth mentioning that to maintain the generality of the present physical model being addressed here, the influence of pressure gradient along the flow direction is ignored. From Figs. 6(a) and 6(b) it can be observed that the axial flow velocity profile is also divided into two regions according to the different magnitudes of Ha as expected. The reason is as follows: there are an aiding electromagnetic body force (SHa) and an retarding term ($Ha^2 u$) which appear in the governing equation (12). When Ha is small ($Ha < 1$), the aiding body force is dominant, resulting in the increase in the axial velocity. With the further increase of Ha ($Ha > 1$), the effect of opposing body force supersedes that of aiding magnetic force, and a decreasing trend can be observed. The value of Ha corresponding to the turning point is called the critical Ha, which has been discussed in Ref. [38]. Meanwhile, we can observe that the total axial velocity increases with normalized electric field strength S increasing, which is a natural result corresponding to the aiding electromagnetic body force (SHa).

Further, the variations of total axial volume flow rate with Ha for different vbalues of non-dimensional slip length δ and the normalized electric field strength S are discussed in Fig. 7. It can be observed that both profiles show an increasing trend with the increase of the values of δ and S for any Ha. We can also observe the fact that the volume flow rate presents increasing–decreasing trend as Ha increases.

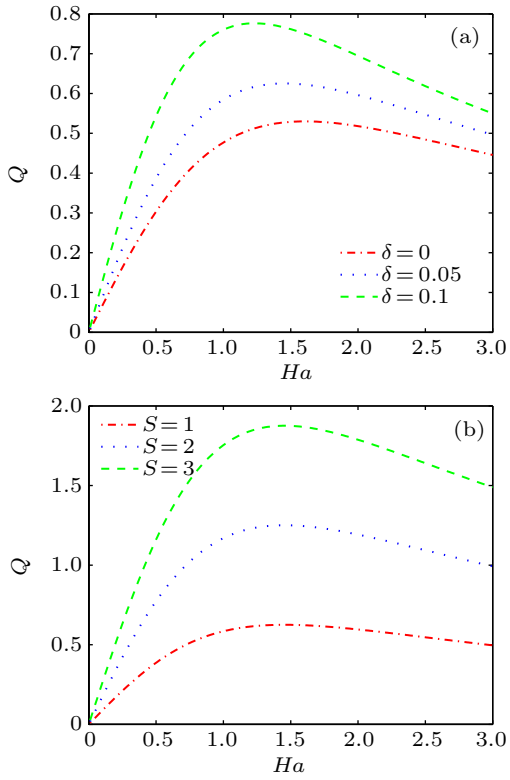


Fig. 7. Variations of total axial volume flow rate with Ha for different values of slip length δ and electric field strength S: (a) $S = 1$ and (b) $\delta = 0.1$ at $x = 0.2096$, $Re = 0.01$, $\Omega = 0$, $K = 1$, and $\alpha = 0.01$.

4. Conclusions

Two-dimensional EMHD flow is investigated under the patterned slip boundary condition. The analytical expression of velocity is obtained by using the perturbation expansion method with consideration of low Reynolds number Re. Besides, in order to validate the accuracy of these analytical solutions, we also compute the numerical solution of velocity by the finite difference method. Results reveal that the total axial velocity and volume flow rate show an increasing-decreasing trend with the increase of Ha and the transverse flows appear when the non-zero slip length is considered. In addition, we

observe that the approximate analytical solution of the first order slip velocity is proportional to the slip length. Meanwhile, the increase of wave-number K can induce a significant transverse velocity when the flow is suppressed in the axial direction.

Generally, mixing in microfluidic flows is a challenging task due to the very low Reynolds numbers in such channels. To achieve good microfluidic mixing, transverse or circulating flows are required. Usually, a transverse flow is induced by the use of patterned slip boundary conditions. Therefore, the research results in our paper are very helpful in the potential applications of microfluidic mixing.

References

[1] Gravesen P, Branebjerg J and Jensen O S 1993 *J. Micromech. Microeng.* **3** 168
[2] Becker H and Gärtner C 2000 *Electrophoresis* **21** 12
[3] Ziaiea B, Baldia A, Leia M, Guc Y and Siegel R A 2004 *Adv. Drug Deliv. Rev.* **56** 145
[4] Nguyen N and Wu Z 2005 *J. Micromech. Microeng*. **15** 1
[5] Ohno K, Tachikawa K and Manz A 2008 *Electrophoresis* **29** 4443
[6] Huang L, *et al.* 2000 *Microsyst. Technol.* **6** 235
[7] Lemoff A V and Lee A P 2000 *Sensor. Actuat. B-Chem.* **63** 178
[8] Zhong J, Yi M and Bau H H 2002 *Sensor. Actuat. A* **96** 59
[9] Nguyen N T 2012 *Microfluid. Nanofluid.* **12** 1
[10] Ho J E 2007 *J. Mar. Sci. Tech.* **15** 315
[11] Jian Y J and Chang L 2015 *AIP Adv.* **5** 057121
[12] Sumaira Afzal, Saleem Asghar and Adeel Ahmad 2017 *Chin. Phys. B* **26** 014704
[13] Jang J and Lee S S 2000 *Sensor. Actuat. A* **80** 84
[14] Jian Y J, Si D Q, Chang L and Liu Q S 2015 *Chem. Eng. Sci.* **134** 12
[15] Wang P J, Chang C Y and Chang M L 2004 *Biosens. Bioelectron.* **20** 115
[16] Karniadakis G, *et al.* 2005 *Microflows and Nanoflows: Fundamentals and Simulation* (Interdisciplinary Applied Mathematics Series)
[17] Li D 2008 *Encyclopedia of Microfluidics and Nanofluidics*, Chapter 778, pp. 948–954
[18] Galea T M and Attard P 2004 *Langmuir* **20** 3477
[19] Tabeling P 2005 *Phys. Today* **59** 58
[20] Priezjev N V, Darhuber A A and Troian S M 2005 *Phys. Rev. E* **71** 041608
[21] Rivero M and Cuevas S 2012 *Sens. Actuat. B-Chem.* **166** 884
[22] Bonaccurso E, Butt H J and Craig V S J 2003 *Phys. Rev. Lett.* **90** 144501
[23] Karakare S, Kar A, Kumar A and Chakraborty S 2010 *Phys. Rev. E* **81** 016324
[24] Barrat J L and Lydéric B 1999 *Phys. Rev. Lett.* **82** 4671
[25] Cécile C, Barrat J L, Lydéric B, *et al*. 2003 *Nat. Mater.* **2** 237
[26] Hendy C, Jasperse M and Burnell J 2005 *Phys. Rev. E* **72** 016303
[27] Zhao C and Yang C 2012 *Electrophoresis* **33** 899
[28] Pereira G G 2009 *J. Non-Newton. Fluid* **157** 197
[29] Mayur M, Chakraborty D, Chakraborty J and Chakraborty S 2012 *Phys. Rev. E* **85** 016315
[30] Zhu Y and Granick S 2002 *Phys. Rev. Lett.* **88** 106102
[31] Cottin-Bizonne C, Cross B, Steinberger A and Charlaix E 2005 *Phys. Rev. Lett.* **94** 056102
[32] Benzi R, Biferale L, Sbragaglia M, Succi S and Toschi F 2006 *J. Fluid Mech.* **548** 257
[33] Harting J, Kunert C and Herrmann H J 2006 *Europhys. Lett.* **75** 328
[34] Molokov S, René Moreau and Moffatt K 2007 *Nagare* **27** 191
[35] Navier C L 1823 *Mem. Acad. R. Sci.* **6** 389
[36] Zhu Y and Granick S 2001 *Phys. Rev. Lett.* **87** 096105
[37] Liu Y P, Jian Y J, Liu Q S and Li F Q 2015 *J. Mol. Liq.* **211** 784
[38] Chakraborty R, Dey R and Chakraborty S 2013 *Int. J. Heat Mass Transfer* **67** 1151